Cancer Research

Dendritic Cells in Tumor-Associated Tertiary Lymphoid Structures Signal a Th1 Cytotoxic Immune Contexture and License the Positive Prognostic Value of Infiltrating CD8$^+$ T Cells

Jérémy Goc[1,2,3], Claire Germain[1,2,3], Thi Kim Duy Vo-Bourgais[1,2,3], Audrey Lupo[1,2,3,4], Christophe Klein[2], Samantha Knockaert[1,2,3], Luc de Chaisemartin[1,2,3], Hanane Ouakrim[1,2,3], Etienne Becht[1,2,3], Marco Alifano[5], Pierre Validire[1,6], Romain Remark[1,2,3], Scott A. Hammond[8], Isabelle Cremer[1,2,3], Diane Damotte[1,2,3,4], Wolf-Herman Fridman[1,2,3,7], Catherine Sautès-Fridman[1,2,3], and Marie-Caroline Dieu-Nosjean[1,2,3]

Abstract

Tumor-infiltrating T cells, particularly CD45RO$^+$CD8$^+$ memory T cells, confer a positive prognostic value in human cancers. However, the mechanisms that promote a protective T-cell response in the tumor microenvironment remain unclear. In chronic inflammatory settings such as the tumor microenvironment, lymphoid neogenesis can occur to create local lymph node–like structures known as tertiary lymphoid structures (TLS). These structures can exacerbate a local immune response, such that TLS formation in tumors may help promote an efficacious immune contexture. However, the role of TLS in tumors has yet to be investigated carefully. In lung tumors, mature dendritic cells (DC) present in tumor-associated TLS can provide a specific marker of these structures. In this study, we evaluated the influence of TLS on the characteristics of the immune infiltrate in cohorts of prospective and retrospective human primary lung tumors ($n = 458$). We found that a high density of mature DC correlated closely to a strong infiltration of T cells that are predominantly of the effector–memory phenotype. Moreover, mature DC density correlated with expression of genes related to T-cell activation, T-helper 1 (Th1) phenotype, and cytotoxic orientation. Lastly, a high density of TLS-associated DC correlated with long-term survival, which also allowed a distinction of patients with high CD8$^+$ T-cell infiltration but a high risk of death. Taken together, our results show how tumors infiltrated by TLS-associated mature DC generate a specific immune contexture characterized by a strong Th1 and cytotoxic orientation that confers the lowest risk of death. Furthermore, our findings highlight the pivotal function of TLS in shaping the immune character of the tumor microenvironment, in promoting a protective immune response mediated by T cells against cancer. *Cancer Res; 74(3); 705–15. ©2013 AACR.*

Introduction

The tumor microenvironment is a complex network of different cell types comprising tumor, stromal, and immune cells, interspersed with blood and lymphatic vessels (1). The immune infiltrate in human tumors is heterogeneous depending on the tumor type and the individual. Several reports have identified tumor-infiltrating T cells directed against tumor-associated antigens, indicative of a spontaneous *in situ* immune response in patients with cancer (2–6). Moreover, a strong association between T-cell density with clinical outcome has been reported in many types of human solid cancer (7–13). More precisely, memory T cells with T-helper 1 (Th1) and cytotoxic orientations seem to represent a predominant T-cell population for prediction of favorable clinical outcome (14). In colorectal cancer, a comparison of the T-cell infiltrate with standard pathologic criteria demonstrated the prognostic power of immune criteria (7, 15, 16). These findings support the proposition that the T-cell infiltrate may serve as a new critical marker to aid in classifying cancers (17). Nevertheless, despite the well-recognized prognostic value of tumor-infiltrating lymphocytes (TIL) in some cancers, mechanisms that govern their recruitment and activation into the tumor remain unclear.

It is generally recognized that secondary lymphoid organs, comprising lymph nodes, spleen, and mucosal-associated lymphoid tissues are the primary site of induction of adaptive immune responses (18). In addition, organized lymphoid aggregates termed tertiary lymphoid structures (TLS) can develop locally, at sites of persistent inflammatory disorders. Lymphoid neogenesis has been described in various human

Authors' Affiliations: [1]Laboratory Immune Microenvironment and Tumors, INSERM U872, Cordeliers Research Center; [2]University Pierre et Marie Curie; [3]University Paris Descartes, UMRS 872; [4]Departments of Pathology and [5]Thoracic Surgery, Hôtel Dieu Hospital, AP-HP; [6]Department of Pathology, Institut Mutualiste Montsouris; [7]Department of Immunology, European Georges Pompidou Hospital, AP-HP, Paris, France; and [8]Oncology Research, MedImmune LLC, Gaithersburg, Maryland

Note: Supplementary data for this article are available at Cancer Research Online (http://cancerres.aacrjournals.org/).

Corresponding Author: Marie-Caroline Dieu-Nosjean, Laboratory Immune Microenvironment and Tumors, UMRS872 INSERM, Cordeliers Research Center, 15 rue de l'école de Médecine, F-75270 Paris, France. Phone: 33-1-44-27-90-86; Fax: 33-1-44-27-81-17; E-mail: mc.dieu-nosjean@crc.jussieu.fr

doi: 10.1158/0008-5472.CAN-13-1342

pathologies, comprising infections, autoimmune diseases, and organ transplant rejections (19–21). TLS exhibit strong structural analogies with canonical secondary lymphoid organs and present features of an ongoing immune reaction site (22–24). Moreover, several studies in mouse models have demonstrated that TLS can induce a protective primary and secondary immune response independently of secondary lymphoid organs during respiratory viral infection (25, 26). However, the potential contribution of TLS to the promotion of an intratumoral immune reaction and their influence on the tumor immune contexture remain poorly investigated.

We have previously reported the presence of TLS in the tumor stroma of early-stage non–small cell lung cancer (NSCLC), composed of clusters of DC-Lamp$^+$ mature dendritic cells (DC; referred as "TLS mature DC") and T cells within T-cell area adjacent to B-cell follicle (27). These structures are surrounded by PNAd$^+$ high endothelial venules (HEV), which are specialized blood vessels mediating lymphocyte extravasation into canonical lymphoid organs (28). Moreover, TLS were associated with a specific set of chemoattractant molecules involved in T-cell homing, suggesting their participation for the immigration of peripheral blood T cells into the tumor (29). In addition, DC-Lamp$^+$ mature DC that home selectively in TLS have been associated with long-term survival in patients with early-stage NSCLC supporting the involvement of TLS in the promotion of a protective immunity (27). We hypothesized that TLS could represent a privileged site for the recruitment and activation of TIL in human lung tumors and aimed to evaluate the potential influence of these structures on the tumor immune contexture.

Here, we investigated the impact of the TLS on the immune contexture in 458 NSCLC comprising all stages of the disease. Using immunohistochemistry, flow cytometry, and quantitative real-time PCR, we demonstrated that TLS mature DC are strongly associated with a specific Th1 and cytotoxic immune signature and a long-term survival. In addition, the combination of mature DC and CD8$^+$ T-cell densities constitutes a powerful and independent prognostic factor for overall survival (OS). Altogether, our data emphasize a major role for TLS in shaping the tumor immune contexture, and support their involvement in the promotion of a protective immune response mediated by T cells.

Patients and Methods

Patients

Fresh ($n = 54$ patients), frozen ($n = 28$ patients), and paraffin-embedded ($n = 376$ patients) primary lung tumor samples were obtained from patients with NSCLC who underwent a complete surgical resection of their lung tumors at Institut Mutualiste Montsouris or Hotel Dieu Hospital (Paris, France). Three hundred seventy-six patients with NSCLC operated between June 15, 2001, and November 26, 2004, were retrieved retrospectively. Patients who received neoadjuvant chemotherapy or radiotherapy were ineligible. The observation time of the cohort was the interval between the surgery and the last contact (last follow-up or death of the patient). At the completion of the study, the minimal clinical follow-up was 90 months for the last patient included in the cohort. The main clinical and pathologic features of the patients enrolled are presented in Table 1 for the retrospective study and in Supplementary Tables S1 and S2 for the prospective study on fresh and frozen tumors (20 common patients between the 2 prospective cohorts), respectively. The data on long-term outcomes

Table 1. Baseline characteristics of the patients with NSCLC enrolled in the retrospective study

Characteristics	Number	%
Gender		
Male/female	302/74	80/20
Age		
Mean (y) ± SEM	62 ± 10	
Range	19–83	
Smoking history		
Current	315	84
Never smokers	52	14
ND	9	2
Pack-years (y) ± SEM	42 ± 24	
Range	0–120	
Histologic type		
ADC	241	64
SCC	111	29
Others	18	5
ND	6	2
Emboli		
No	141	37
Yes	210	56
ND	25	7
pT stage		
T1	85	22
T2	180	48
T3	84	22
T4	25	7
ND	2	1
pN stage		
N0	239	64
N1	67	18
N2	66	17
ND	4	1
pTNM stage		
I	167	44
II	101	27
III	104	28
IV	2	0.5
ND	2	0.5
Vital status of patients		
Alive	146	39
Dead	230	61

NOTE: All parameters were evaluated among 376 patients with NSCLC.

Abbreviations: ADC, adenocarcinoma; ND, not done; pT, pathologic T stage; pN, pathologic N stage.

were obtained retrospectively by interrogation of municipality registers or the family of patients. A written informed consent was obtained from the patients before inclusion in the prospective study. The protocol was approved by the local ethics committee (nos. 2008-133 and 2012-0612) in application with the article L.1121-1 of French law.

Immunohistochemistry and immunofluorescence

For each paraffin-embedded lung tumor, two observers (one expert pathologist and one investigator trained to identify the pathologic features of NSCLC) selected the tumor section containing a representative area of tumor with adjacent lung parenchyma, and the highest density of immune cells on the hematoxylin and eosin-safran–stained tissue section. Briefly, serial 5-μm tissue sections were deparaffinized, rehydrated, and pretreated in appropriate buffer for antigen retrieval. The sections were incubated with 5% human serum for 30 minutes before adding the appropriate primary antibodies followed by secondary antibodies (see Supplementary Table S3). Enzymatic activity was performed as described (27). For single staining, sections were counterstained with hematoxylin. Images were acquired using a Nanozoomer (Hamamatsu) operated with NDPview software.

Method for cell quantification

The quantification of DC-Lamp$^+$ DC was determined as previously described (27). CD8$^+$ cells were enumerated in the tumor nests and the stroma of the whole tumor section with Calopix software (Tribvn), and expressed as an absolute number of positive cells/mm^2 of the areas of interest. Both immunostaining and quantification were reviewed by at least two independent observers (J. Goc, and R. Remark, T.K.D. Vo-Bourgais or M.-C. Dieu-Nosjean).

Flow cytometry

Fresh lung tumor specimens were mechanically (manual) dissociated and digested in the presence of Cell Recovery Solution (BD Biosciences) instead of enzymes that can remove CCR7 and CD62L at the cell surface. Then, total live mononuclear cells were isolated from the tumors, as previously described (29). Mononuclear cells were stained with multiple panels of antibodies conjugated to fluorescent dyes (see Supplementary Table S3). Briefly, after saturation with 2% human serum, mononuclear cells were incubated with the primary antibodies or appropriate isotype controls for 30 minutes at 4°C in the dark. Cells were washed and fixed in 0.5% formaldehyde before the analysis on a LSRII or Fortessa cytometer (BD Biosciences). Flow cytometry data were analyzed with the Diva (BD Biosciences) and FlowJo (TreeStar, Inc.) softwares. The gating strategies are explained in Supplementary Fig. S1.

RNA extraction and reverse transcription

Total RNA from frozen tissues was extracted with the RNeasy Mini Kit (Qiagen) according to the manufacturer's instructions, and RNA quantity and quality were determined with 2100 Bioanalyzer (Agilent Technologies). Samples with a RNA integrity number $\geq$7 were reverse transcribed into cDNA using the High Capacity cDNA Kit (Life Technologies) according to the manufacturer's instructions.

Quantitative PCR

Complementary DNA samples were amplified using the Low Density Array System according to the manufacturer's instructions (Applied Biosystems). The arrays (Human Immune Array; TaqMan) were processed on a TaqMan 2900HD (Life Technologies). Four nanograms of cDNA per qRT-PCR was used. Expression levels of genes were determined using threshold cycle (Ct) values normalized to *β-actin* expression as an endogenous control (ΔCt).

Statistical analysis

We used the Mann–Whitney test to compare the density of infiltrating immune cells in the different tumors. Correlations were performed using the Spearman test. OS curves were estimated by the Kaplan–Meier method and differences between the groups of patients were calculated using the log-rank test. The start of follow-up for OS was the time of surgery. Together with mature DC and CD8$^+$ cell densities, the following available clinical parameters were tested: tumor–node–metastasis (TNM) stage according to the new classification 2009 (30), smoking history, histologic type according to the classification of the WHO (31), intervention type and emboli. With respect to immune cell densities, the "minimum *P* value" approach was used to determine the cutoff (Supplementary Fig. S2) for the best separation of patients referring to their OS outcome (outcome-oriented approach). Optimal cutoff values are 1.964, 383, and 114 cells per mm^2 for DC-Lamp$^+$, CD8$_S$, and CD8$_T$ cells, respectively. Because the *P* values obtained might be underestimated, OS log-rank *P* values were corrected using the formula proposed by Altman and colleagues (32) and validated using 100 repetitions of 2-fold cross-validations. We have also ensured that the significance established at the optimal cutoff remained valid at the quartiles (Supplementary Table S4). A *P* value of less than 0.05 was considered statistically significant. Parameters identified at univariate analysis as possibly influencing the outcome ($P < 0.05$) were introduced in a multivariate Cox-proportional hazards regression model. All analyses were performed with Prism 5 (GraphPad), Statview (Abacus Systems), and R (http://www.r-project.org/). Correlation matrix was represented with the Genesis software (Institute for Genomics and Bioinformatics, Gratz, Austria; ref. 33).

Results

Mature DC density is associated with early-differentiated and intermediate effector–memory CD8$^+$ T-cell infiltration in human lung tumors

We performed large-scale flow cytometry analyses on 54 freshly resected human NSCLC to characterize the immune infiltrate according to the density of DC-Lamp$^+$ mature DC (Fig. 1). We observed a significant higher percentage of total CD3$^+$, CD3$^+$CD4$^+$, and CD3$^+$CD8$^+$ T cells, a nonsignificant trend for CD19$^+$ B cells and no difference for CD3$^-$CD56$^+$

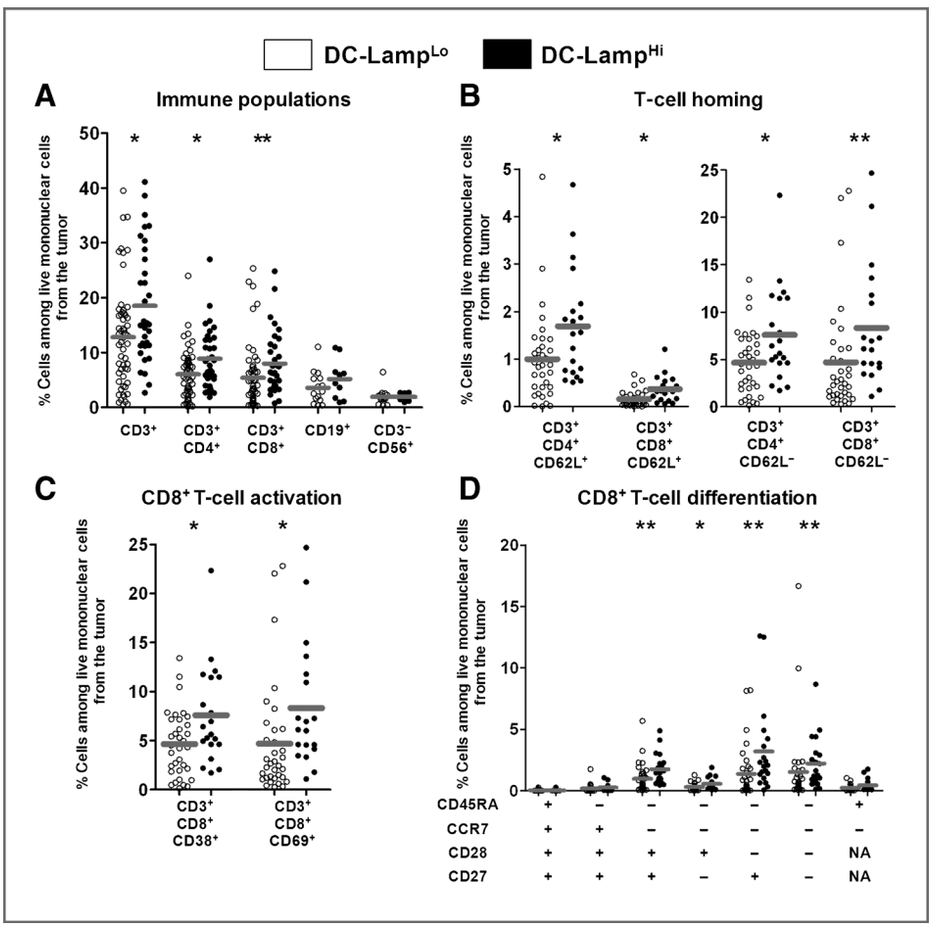

Figure 1. Phenotypic analysis of the immune cell infiltrate according to the high and low density of mature DC. Large-scale flow cytometry analysis of immune cell populations stratified by the density of mature DC in 54 fresh lung tumors (34 DC-Lamp^{Lo} tumors vs. 20 DC-Lamp^{Hi} tumors). Density of mature DC was evaluated by immunohistochemistry. The percentage of the different cell types among total live mononuclear cells from the tumors of DC-Lamp^{Lo} (white circles) and DC-Lamp^{Hi} (black circles) is shown. A, percentage of total CD3$^+$ T cells, CD4$^+$ and CD8$^+$ T-cell subsets, CD19$^+$ B cells, and CD56$^+$CD3$^-$ NK cells in groups of DC-Lamp^{Hi} tumors versus DC-Lamp^{Lo} tumors. B, proportion of CD3$^+$ CD4$^+$ and CD3$^+$ CD8$^+$ T-cell subsets expressing either CD62L$^+$ or CD62L$^-$ T cells in DC-Lamp^{Hi} versus DC-Lamp^{Lo} tumors. C and D, proportion of CD3$^+$ CD8$^+$ T cells expressing the activation markers CD38 and CD69 (C) with effector–memory phenotype (D) among groups of DC-Lamp^{Hi} versus DC-Lamp^{Lo} tumors. *, $P < 0.05$; **, $P < 0.01$; Mann–Whitney *U* test. NA, not applicable.

natural killer (NK) cells (Fig. 1A) among total live mononuclear cells from the tumor between patients with a high density of DC-Lamp$^+$ DC (DC-Lamp^{Hi} patients) versus patients with a low density of DC-Lamp$^+$ DC (DC-Lamp^{Lo} patients). DC-Lamp^{Hi} tumors had a significantly greater amount of CD62L$^+$CD4$^+$ and CD62L$^+$CD8$^+$ T cells than DC-Lamp^{Lo} tumors (Fig. 1B, left), in accordance with the selective localization of CD62L$^+$ T cells inside the TLS (Supplementary Fig. S3; ref. 29). We also observed a significant and concomitant increase of antigen-experienced CD62L$^-$CD4$^+$ and CD62L$^-$ CD8$^+$ T cells, which represent the majority of TIL among total mononuclear cells (Supplementary Fig. S4A), between DC-Lamp^{Hi} versus DC-Lamp^{Lo} tumors (Fig. 1B, right). Interestingly, a positive correlation was observed between the proportion of CD62L$^+$ and CD62L$^-$ T-cell subsets among total live mononuclear cells in the tumors (Supplementary Fig. S4B).

As compared with DC-Lamp^{Lo} tumors, DC-Lamp^{Hi} tumors were more infiltrated by activated CD38$^+$ or CD69$^+$ CD8$^+$ T cells (Fig. 1C) and by the four main subpopulations of effector–memory CD8$^+$ T cells (CD45RA$^-$CCR7$^-$CD27$^{+\text{ or }-}$CD28$^{+\text{ or }-}$; Fig. 1D) whereas no difference was seen for terminally differentiated effector–memory T cells (also called TEM-RA), which were detected at a very low frequency.

Altogether, these results demonstrate that DC-Lamp^{Hi} tumors have higher numbers of TLS T cells, as well as a higher number of activated and effector–memory non-TLS T cells, than DC-Lamp^{Lo} tumors.

Density of mature DC signals a coordinated *in situ* Th1, cytotoxic, and activated T-cell immune reaction

Because the density of mature DC that home selectively in TLS is associated with an increased number of TIL, we next evaluated the impact of TLS on the functional characteristics of the immune cell infiltrate with a focus on T lymphocytes. Gene expression levels related to the main immune populations, TLS, Th1 and T-helper 2 (Th2) orientations, CD8$^+$ T-cell cytotoxicity, T-cell activation, immunosuppression, inflammation, and angiogenesis were assessed in whole frozen tumors from 14 patients with DC-Lamp^{Hi} tumors, and compared with 14 patients with DC-Lamp^{Lo} tumors (Fig. 2A, Supplementary Fig. S5, and Supplementary Tables S2 and S5). As a control, genes related to the TLS cluster (*CCL19, CCR7, CD28, CD62-L*, and *lymphotoxin-α*) were significantly overexpressed among DC-Lamp^{Hi} versus DC-Lamp^{Lo} tumors ($P = 0.0006$). DC-Lamp^{Hi} tumors and not DC-Lamp^{Lo} tumors were also associated with the overexpression of sets of genes clustered into specific groups: immune cell populations ($P = 0.0011$), Th1 polarization ($P = 0.0002$), CD8$^+$ T-cell cytotoxicity ($P = 0.0013$), and T-cell activation ($P = 0.0005$). Most of these molecules were detected at the protein level by

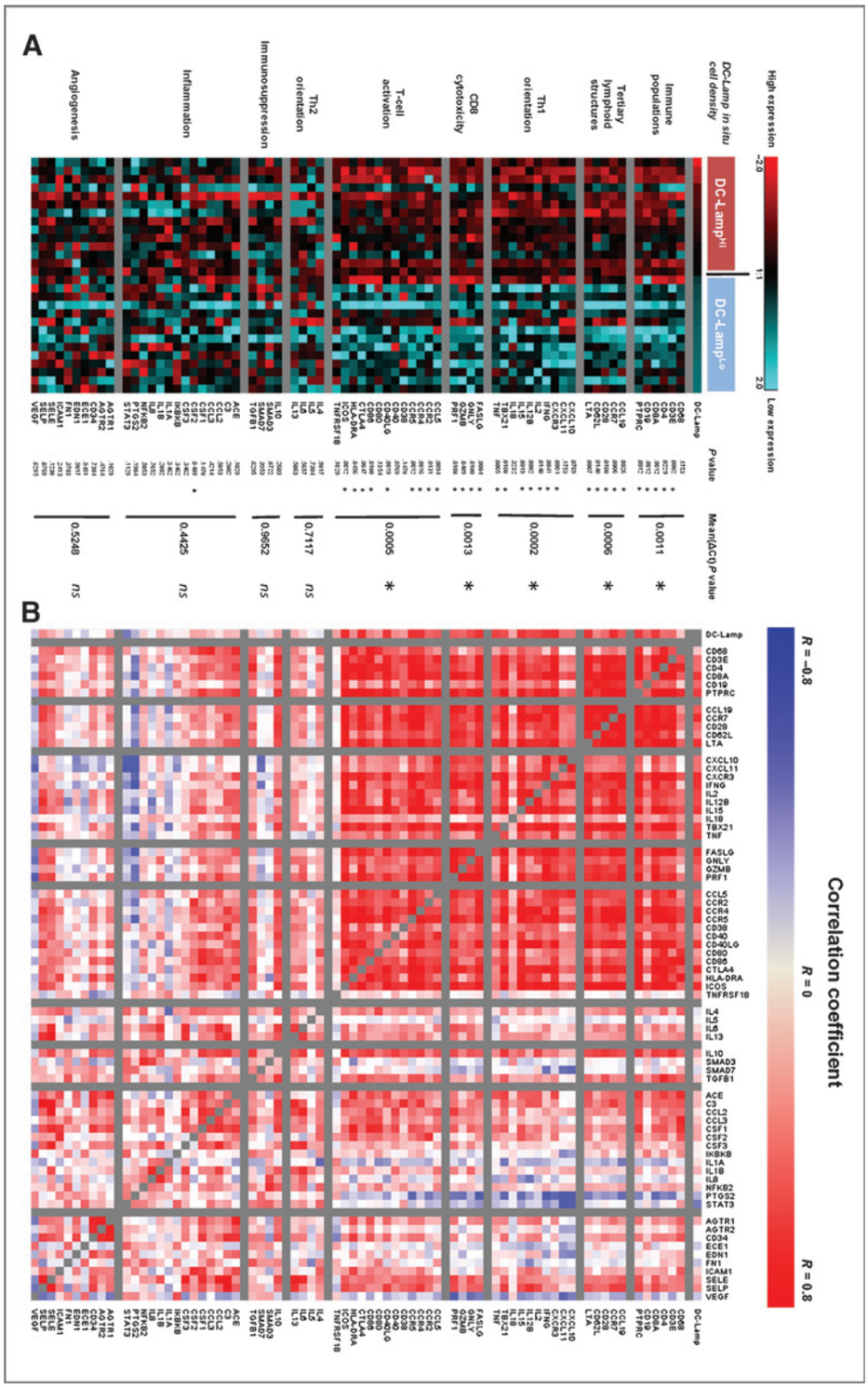

Figure 2. Gene expression levels related to immune populations, TLS, Th-orientation, cytotoxicity, T-cell activation, immunosuppression, inflammation, and angiogenesis according to the high and low density of mature DC. Gene expression levels were assessed by qRT-PCR and determined using threshold cycle (Ct) values normalized (ΔCt) to the *actin* housekeeping gene ($n = 28$ frozen lung tumor samples). The heat map representation of clusters of genes related to immune populations, TLS, Th1 and Th2 orientation, cytotoxicity, T-cell activation, immunosuppression, inflammation, and angiogenesis is shown in A. Genes are plotted from the minimal level of expression (blue) to the maximal level (red). Density of mature DC was evaluated by immunohistochemistry. Comparison of gene expression levels between DC-Lamp^{Hi} versus DC-Lamp^{Lo} patient groups was performed using the Mann–Whitney test. A correlation matrix was constructed with the same genes. Each square in B represents a Spearman correlation coefficient (blue, negative correlation; red, positive correlation).

immunohistochemistry and/or by flow cytometry on T cells: immune cells (Figs. 1 and 3; ref. 1), TLS signature (Fig. 1; ref. 29), Th1 orientation (Supplementary Fig. S6; ref. 27), chemokine receptors (29), and T-cell cytotoxicity and activation (Supplementary Fig. S6).

In contrast, genes involved in Th2 polarization, immunosuppression, inflammation (excepting *CSF-2*), and angiogenesis were not differentially expressed between the two groups of patients (Fig. 2A). We constructed a correlation matrix and demonstrated that the expression of all genes overexpressed

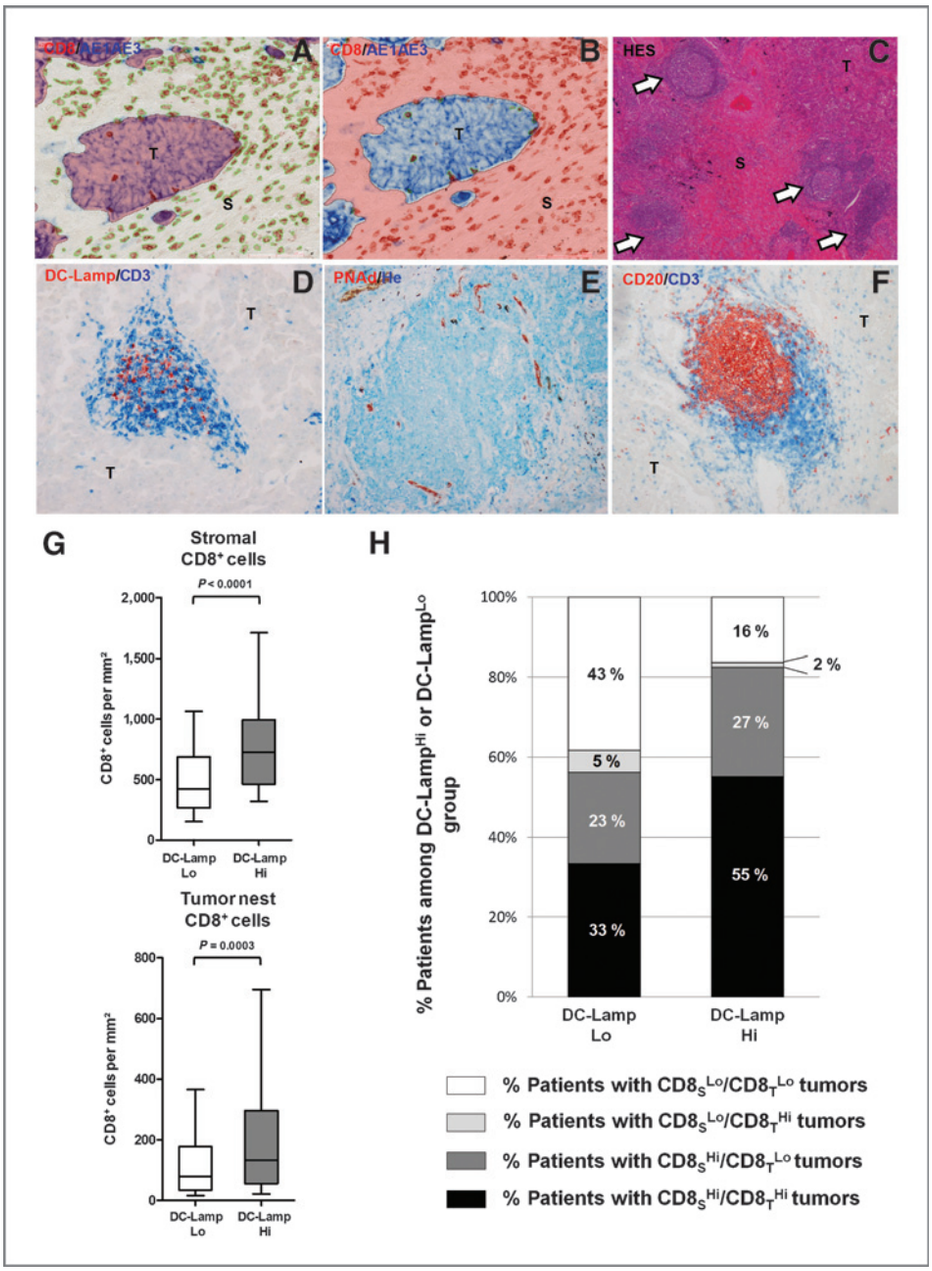

Figure 3. Analysis of the distribution of $CD8_T$ and $CD8_S$ positive cells in DC-$Lamp^{Hi}$ versus DC-$Lamp^{Lo}$ patients. Immunostainings were performed on 376 paraffin-embedded tumor samples. Notice that $CD8^+$ cells (red cells surrounded by a green line) were counted selectively in the stroma (A) and pan-cytokeratins$^+$ tumor nests (B, blue cells stained with AE1/AE3 antibodies). TLS are detected by immunohistochemistry in NSCLC counterstained with hematoxylin and eosin (HES; C). TLS are composed by T-cell–rich areas that comprised DC-$Lamp^+$ DC (D; red) in contact with $CD3^+$ T cells (blue). E, TLS are surrounded by $PNAd^+$ HEV (red). He, hematoxylin. F, the $CD3^+$ T-cell zone (blue) is adjacent to $CD20^+$ B-cell follicles (red). Lower magnification of immunohistochemistry stainings is shown in Supplementary Fig. S8. Quantification of positive cells was performed on the whole section. G, distribution of the density of $CD8_T$ (left) and $CD8_S$ (right) T cells among groups of DC-$Lamp^{Lo}$ (white bars) versus DC-$Lamp^{Hi}$ tumors (gray bars). Statistical significance was calculated by the Mann–Whitney test. H, DC-$Lamp^{Hi}$ and DC-$Lamp^{Lo}$ patients stratified by high or low density of $CD8_S$ and $CD8_T$ cells.

among DC-$Lamp^{Hi}$ tumors (immune cell subsets: *CD3, CD4, CD8, CD20*; TLS: *CCL19, CCR7, CD28, CD62L*, and *LTA*; Th1 orientation: *CXCR3, IFN-γ, interleukin (IL)-2, IL-12B, IL-15, T-bet*, and *TNF-α;* cytotoxicity: *FAS-L, GNLY, GZMB,* and *PRF1*; and T-cell activation: *CCL5, CCR2, CCR4, CCR5, CD40L, CD86, CTLA-4, HLA-DRα*, and *ICOS*) was also significantly correlated (correlation coefficient in Fig. 2B, and *P* value in Supplementary Fig. S7A and S7B).

Altogether, these results demonstrate that mature DC density correlates with a specific intratumoral immune contexture characterized by the overexpression and coordination of genes related to T-cell activation, Th1 orientation, and cytotoxic effector functions.

High density of mature DC predicts high levels of $CD8^+$ T-cell infiltration in lung tumors

A correlation between $CD8^+$ T-cell infiltration and a favorable clinical outcome was previously reported in many types of human solid cancer (8, 9, 13–15). As we observed a close association between mature DC density with cytotoxic effector function, we further investigated the relationship between mature DC and $CD8^+$ T-cell infiltration. Because $CD8^+$ T cells are expected to establish a contact with tumor cells to exert their cytolytic function, we discriminated $CD8^+$ T cells present in the tumor nests and in the stroma in the following analysis.

In a retrospective series of 376 patients with NSCLC (Table 1), we quantified stromal $CD8^+$ T cells ($CD8_S$), tumor nest

$CD8^+$ T cells ($CD8_T$), and mature DC-$Lamp^+$ DC (Fig. 3A, B, and D). As previously observed in early-stage lung tumors (27), we confirmed that mature DC home selectively in the T-cell–rich areas of TLS (Fig. 3C and D) adjacent to $PNAd^+$ vessels and B-cell follicles (Fig. 3E and F) in all stage lung tumors.

In accordance with the results above, we observed a higher density of both $CD8_T$ and $CD8_S$ cells (Fig. 3G) among DC-$Lamp^{Hi}$ versus DC-$Lamp^{Lo}$ tumors (mean = 254 vs. 138 $CD8_T/mm^2$, $P = 0.0003$; mean = 843 vs. 553 $CD8_S/mm^2$, $P < 0.0001$, respectively). Consequently, substratification of DC-$Lamp^{Hi}$ and DC-$Lamp^{Lo}$ patients according to $CD8_S$ and $CD8_T$ cell densities revealed that 84% of DC-$Lamp^{Hi}$ patients were $CD8^{Hi}$ in at least one region, and in particular 55% were high in both regions (Fig. 3H). These proportions were reduced in DC-$Lamp^{Lo}$ patients with 61% of $CD8^{Hi}$ in at least one region, and only 33% in both regions. Interestingly, patients with $CD8_S{}^{Lo}/CD8_T{}^{Hi}$ tumors were rare in both DC-Lamp groups, in accordance with the trafficking of infiltrating T cells from the stroma to the tumor nests. The main differences between DC-$Lamp^{Hi}$ versus DC-$Lamp^{Lo}$ patients concerned the percentage of $CD8_S{}^{Hi}CD8_T{}^{Hi}$ and $CD8_S{}^{Lo}CD8_T{}^{Lo}$ patients whereas the percentages of mix groups ($CD8_S{}^{Hi}CD8_T{}^{Lo}$ and $CD8_S{}^{Lo}CD8_T{}^{Hi}$) were quite unchanged. There were no distinguishable clinical characteristics [except for gender, histologic type, and pathologic TNM (pTNM) stage] between the patients with DC-$Lamp^{Hi}$ versus DC-$Lamp^{Lo}$ tumors (Supplementary Table S6). The gender and histologic type are also correlated, as most females were diagnosed with a squamous cell carcinoma (SCC; adenocarcinoma, SCC, and other types: 85%, 11%, and 4% of females, and 59%, 34%, and 7% of males, respectively, $P = 0.0026$). This observation may, in part, explain the differential distribution of gender and histologic type among the groups of DC-$Lamp^{Hi}$ versus DC-$Lamp^{Lo}$ patients. Using Cox multivariate regression analyses, we demonstrate that pTNM stage and DC-Lamp density were two independent prognostic factors (Supplementary Table S7).

Altogether, these results demonstrate that a high density of mature DC is closely related to a strong $CD8^+$ T-cell infiltration.

Density of TLS DC allows the identification of $CD8^{Hi}$ and $CD8^{Lo}$ patients with high risk of death

Because we observed that high densities of $CD8^+$ T cells were detected in both groups of DC-$Lamp^{Hi}$ and DC-$Lamp^{Lo}$ patients, we next evaluated the prognostic value of each variable alone and in combination (Fig. 4).

The Kaplan–Meier curves indicate that the densities of mature DC ($P = 9.1 \times 10^{-05}$; Fig. 4A), $CD8_S$ cells ($P = 0.0019$; Fig. 4B), and $CD8_T$ cells ($P = 0.0228$; Fig. 4C) were correlated with longer OS.

Because the presence of mature DC and $CD8^+$ cells in the tumors positively influence the outcome of patients with lung cancer, we stratified the patients into four groups according to the high or low density of each marker (DC-$Lamp^{Hi}/CD8^{Hi}$, DC-$Lamp^{Hi}/CD8^{Lo}$, DC-$Lamp^{Lo}/CD8^{Hi}$, and DC-$Lamp^{Lo}/CD8^{Lo}$; Fig. 4D). We observed that the group of patients with DC-$Lamp^{Hi}$ tumors regardless of the density of $CD8_S$ cells had the lowest risk of death ($P = 3.4 \times 10^{-07}$, median OS were 92 months for DC-$Lamp^{Hi}/CD8_S{}^{Hi}$ patients and 100 months for DC-$Lamp^{Hi}/CD8_S{}^{Lo}$ patients), as was observed for DC-$Lamp^{Hi}$ patients (Fig. 4A). Interestingly, only the DC-$Lamp^{Hi}$ patients present an improved survival as compared with the whole cohort. In contrast, patients with a low density of both dendritic cells (DC) and $CD8_S$ cells were at highest risk of death (median OS was 22 months) as compared with each immune marker alone (median OS: DC-$Lamp^{Lo}$ = 36 months, $CD8_S{}^{Lo}$ = 40 months). Patients with DC-$Lamp^{Lo}/CD8_S{}^{Hi}$ tumors were at an intermediate risk of death (median OS = 41 months). Same results were obtained when the analysis was performed on the combination of DC-Lamp with $CD8_T$ cells (data not shown). Additional analyses with 100 repetitions of 2-fold cross-validations confirmed the high and significant prognostic value of DC-Lamp/$CD8_S$ score (cross-validated 99/100 tests, median P value $= 4.7 \times 10^{-04}$). Using Cox multivariate regression analyses (Table 2), the pTNM stage and DC-Lamp/$CD8_S$ score were the only criteria significantly and independently associated with OS (HR = 1.70 and 0.71, and $P = 2.83 \times 10^{-07}$ and 4.50×10^{-07}, respectively).

All together, these data demonstrate that DC-Lamp alone is a good marker for the identification of patients with a favorable outcome whereas the combination of CD8 with DC-Lamp allows the identification of patients with the highest risk of death. Finally, the DC-Lamp/$CD8_S$ score and pTNM stage constitute two independent and powerful prognostic factors.

Discussion

The major clinical impact of TIL has emphasized the need to better identify the mechanisms underlying their recruitment and activation (14). Based on the structural analogy with lymph nodes, we hypothesized that lung tumor TLS could play a key role in the promotion of a local immune reaction. The ability of TLS to promote an efficient and protective T-cell response in many chronic inflammatory contexts (19–21) provided the rationale for this study.

By combining immunohistochemical and bio-molecular analyses, we demonstrated that a high density of TLS mature DC is associated with a specific immune orientation characterized by the overexpression and coordination of genes related to T-cell activation, Th1 polarization, and cytotoxic effector functions. By contrast, immune genes related to Th2 polarization, immunosuppression, inflammation, and angiogenesis were not differentially expressed between groups of patients with high or low densities of TLS mature DC. In agreement with these results, previous reports have also demonstrated that TLS correlated with an increased number of T-bet^+ lymphocytes or high levels of cytotoxic gene expression in NSCLC and colorectal cancers, respectively (27,34). This specific Th1 and cytotoxic orientation related to mature DC density suggests a major influence of TLS mature DC in the shaping of the tumor immune contexture.

The significant increase of T-cell proportion, comprising $CD62L^+$ T cells among the group of DC-$Lamp^{Hi}$ versus DC-$Lamp^{Lo}$ tumors, is in agreement with the selective presence of $CD62L^+$ T cells located close to $PNAd^+$ HEV (and vice versa) in TLS (29). Interestingly, a crucial role for DC in the maturation

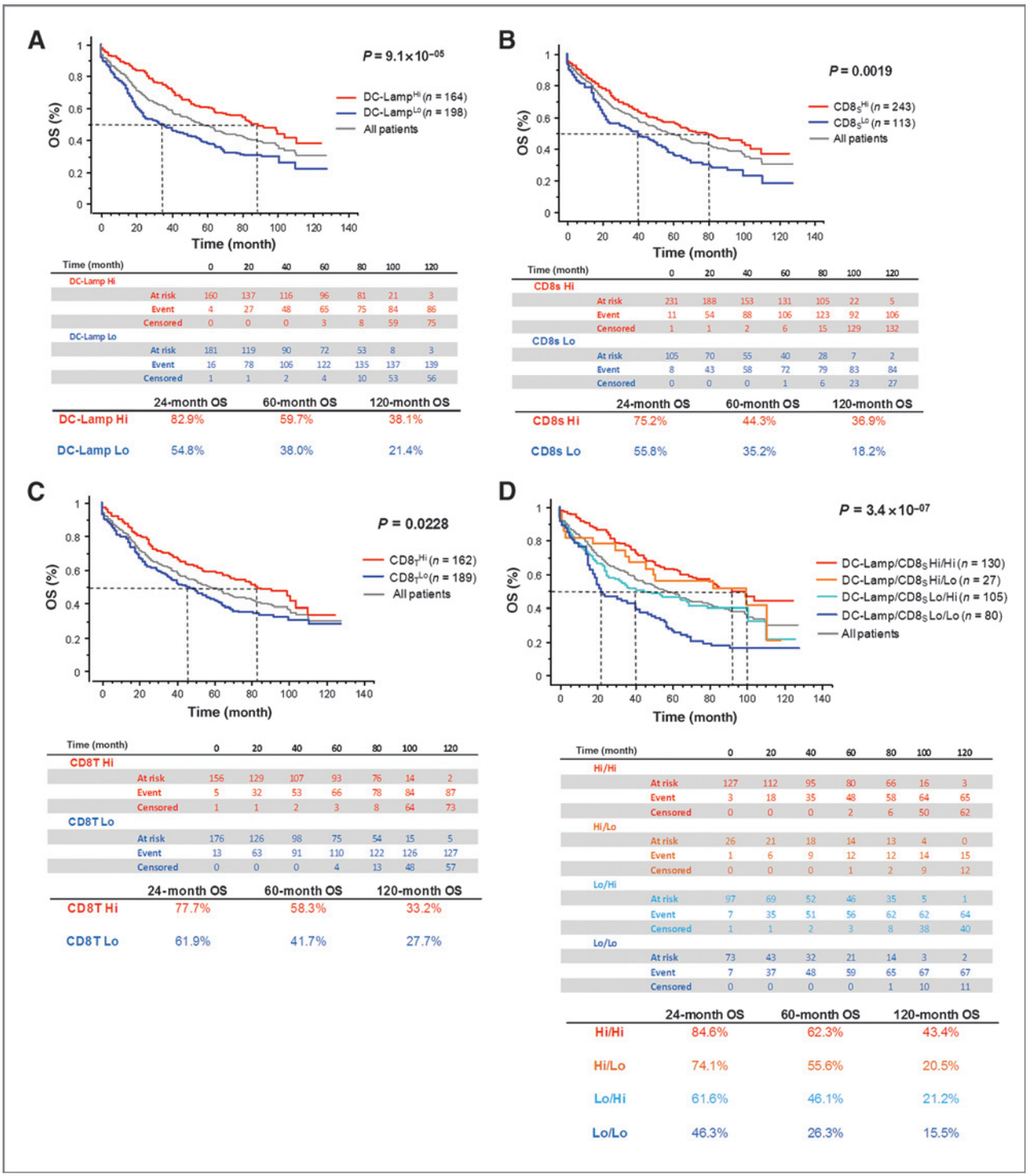

Figure 4. Overall survival for patients with NSCLC according to the presence of a high or low density of DC-Lamp$^+$ mature DC (A), $CD8_S$ cells (B), and $CD8_T$ cells (C), or both DC-Lamp$^+$ DC and $CD8_S$ cells (D). OS curves for patients with NSCLC were estimated by the Kaplan–Meier method, and differences between groups of patients were evaluated using the log-rank test. Tables show the number of events, censored and at-risk patients according to the cell density group. Tables show the 24-month, 60-month, and 120-month OS rates (%) according to the group of patients, respectively.

of HEV (35) and maintenance of TLS (22, 23) has been demonstrated in mice. In addition, close correlations between the density of HEV and lymphocyte infiltrate have been reported in melanoma (36, 37), human breast cancer (38), and in the methylcholanthrene-induced fibrosarcoma mouse model (39), which argue for functional features of HEV in tumor microenvironment. Altogether, these data strongly support that intratumoral HEV mediate recruitment of CD62L$^+$ T cells

Table 2. Multivariate Cox proportional hazards analysis for overall survival in patients with NSCLC

Variable	PHA test	HR	95% CI	*P*
Intervention type (lobectomy vs. pneumonectomy)	0.200	1.5	0.98–2.23	0.0629
Emboli (no vs. yes)	0.489	1.35	0.95–1.90	0.0901
pTNM stage 2009	0.171	1.70	1.39–2.08	2.83e−07
DC-Lamp/$CD8_S$ densities	0.278	0.71	0.62–0.81	4.50e−07

NOTE: All parameters were evaluated among 325 patients with NSCLC. Patients were stratified into four groups according to the high/low densities of mature DC and stromal $CD8^+$ cells (DC-$Lamp^{Hi}$/$CD8^{Hi}$, DC-$Lamp^{Lo}$/$CD8^{Hi}$, DC-$Lamp^{Hi}CD8^{Lo}$, and DC-$Lamp^{Lo}$ $CD8^{Lo}$). All categorical variables were transformed into discrete numeric variables before they were added into the Cox model. PHA test, $P < 0.05$, violates the proportional hazards assumption.

Abbreviations: CI, confidence interval; PHA, proportional hazards assumption.

from the blood into TLS, which could represent a major gateway for T cells into the tumor.

The density of TLS mature DC is also associated with a strong infiltration of experienced $CD62L^-$ T cells that are predominantly of the effector–memory phenotype. These experienced T cells may derive, in part, from TLS $CD62L^+$ T cells, which have undergone a local activation and differentiation. Studies in mouse models indicated that TLS could play a key role in the induction of a local immune response. Development of TLS was associated with the generation of specific $CD8^+$ T cells and viral clearance in mice lacking secondary lymphoid organs (19, 20). A recent study also demonstrated that the activation, expansion, and differentiation of naïve $CD8^+$ T cells into effector cells could occur directly in the tumors of mice with B16 melanoma and devoid of secondary lymphoid organs (40). These data highlight that extranodal activation of TIL is possible and can generate an immune response against the tumor independently of a response initiated in canonical lymphoid organs. Furthermore, *de novo* priming of tumor-infiltrating $CD8^+$ naïve T cells has been described in TLS induced by modified vaccine virus Ankara demonstrating that these structures represent a major site for T-cell priming (23). Strikingly, induction of lymphoid neogenesis in tumors manipulated to express LIGHT (lymphotoxins, inducible expression, competes with HSV glycoprotein D for HVEM, expressed by T cells) or lymphotoxin-α generates a massive infiltration of naïve T cells, followed by T-cell activation, expansion, and tumors rejection (41, 42). Altogether, these data underline that TLS may serve as an important site for priming TIL during the generation of a local immune response.

Three major studies have previously reported strong associations between $CD8^+$ T-cell infiltrate with the outcome of patients with lung cancer (9, 43, 44). In agreement with these data and similar results in many other types of cancers (8, 13–15), we found a strong correlation between $CD8^+$ cell density and improved clinical outcome in patients with NSCLC. Compared with our first study performed in patients with early-stage NSCLC (27), we confirmed that mature DC density is still a favorable prognostic biomarker for patient survival (cohort of patients with stages I to IV NSCLC). Interestingly, patients with DC-$Lamp^{Hi}$/$CD8^{Lo}$ tumors were scarce, arguing for a causal link between TLS and $CD8^+$ cells density in which TLS would be an active site for $CD8^+$ T-cell proliferation. More importantly among $CD8^{Hi}$ patients, those with a concomitant DC-$Lamp^{Hi}$ density had a significant clinical benefit as compared with patients with no or few TLS. Thus, DC-Lamp represents a new marker allowing the identification of $CD8^{Hi}$ patients with elevated risk of death, and the combination of both variables allows the identification of a worst-risk group (DC-$Lamp^{Lo}$/$CD8^{Lo}$ patients).

TLS could potentiate an antitumor $CD8^+$ T-cell response in multiple ways. We previously reported that TLS T cells consisted primarily of $CD4^+$ T cells (27, 29). Interestingly, a major role of $CD4^+$ T-cell help for the recruitment, activation, and effector functions of naïve $CD8^+$ T cells was demonstrated in a model of pancreatic tumors (45). This is consistent with the strong coordination between mature DC infiltration, Th1 polarization, T-cell activation, and cytotoxic orientation that we report in this study.

We speculate that TLS mature DC could present tumor-associated antigens that will promote continuous generation of specific T cells directly in the tumor. As a result, TLS could induce a local immune reaction that would be more adaptable to the shifting expression of tumor-associated antigens during tumor progression. A major challenge will now be to characterize and to compare the specificity of experienced T cells according to DC density to evaluate a potential association between TLS and clonal diversity of TIL.

Altogether, our results suggest that TLS represent a privileged area for T-cell recruitment and activation in the primary site of lung tumor, which could play a major role in the shaping of a tumor immune contexture with survival benefit. Lymphoid neogenesis could represent a major phenomenon to promote a protective immune response in lung or other types of cancer, which may provide new opportunities to improve immunotherapy strategies.

Disclosure of Potential Conflicts of Interest

S.A. Hammond is an employee of MedImmune LLC/AstraZeneca and has ownership interest in AstraZeneca. No potential conflicts of interest were disclosed by the other authors.

Authors' Contributions

Conception and design: J. Goc, L. de Chaisemartin, S.A. Hammond, C. Sautès-Fridman, M.-C. Dieu-Nosjean

Development of methodology: J. Goc, T.K.D. Vo-Bourgais, C. Klein, L. de Chaisemartin, D. Damotte, M.-C. Dieu-Nosjean
Acquisition of data (provided animals, acquired and managed patients, provided facilities, etc.): J. Goc, T.K.D. Vo-Bourgais, A. Lupo, S. Knockaert, H. Ouakrim, M. Alifano, P. Validire, R. Remark, D. Damotte
Analysis and interpretation of data (e.g., statistical analysis, biostatistics, computational analysis): J. Goc, T.K.D. Vo-Bourgais, L. de Chaisemartin, E. Becht, S.A. Hammond, M.-C. Dieu-Nosjean
Writing, review, and/or revision of the manuscript: J. Goc, C. Germain, H. Ouakrim, S.A. Hammond, I. Cremer, W.-H. Fridman, C. Sautès-Fridman, M.-C. Dieu-Nosjean
Administrative, technical, or material support (i.e., reporting or organizing data, constructing databases): J. Goc, C. Germain, T.K.D. Vo-Bourgais, H. Ouakrim, P. Validire, D. Damotte, M.-C. Dieu-Nosjean
Study supervision: M.-C. Dieu-Nosjean

Acknowledgments

The authors thank Patricia Bonjour for technical assistance and Martine Bovet for help in clinical data collection. They also thank Estelle Devevre and Helene Fohrer-Ting from the "Centre d'Imagerie Cellulaire et de Cytométrie" (Cordeliers Research Center, Paris) for excellent technical assistance and support in flow cytometry.

Grant Support

This work was supported by the "Institut National de la Santé et de la Recherche Médicale," the "Fondation ARC pour la recherche sur le cancer," the "Cancéropôle Ile-de-France," Université Paris-Descartes, Université Pierre et Marie Curie, Institut National du Cancer (2011-1-PLBIO-06-INSERM 6-1, PLBIO09-088-IDF-KROEMER), CARPEM (Cancer Research for Personalized Medicine), Labex Immuno-Oncology (LAXE62_9UMRS872 FRIDMAN), and MedImmune LLC.

The costs of publication of this article were defrayed in part by the payment of page charges. This article must therefore be hereby marked *advertisement* in accordance with 18 U.S.C. Section 1734 solely to indicate this fact.

Received May 9, 2013; revised November 7, 2013; accepted November 23, 2013; published OnlineFirst December 23, 2013.

References

1. Sautès-Fridman C, Cherfils-Vicini J, Damotte D, Fisson S, Fridman WH, Cremer I, et al. Tumor microenvironment is multifaceted. Cancer Metastasis Rev 2011;30:13–25.
2. Finn OJ. Immunological weapons acquired early in life win battles with cancer late in life. J Immunol 2008;181:1589–92.
3. Parmiani G, Filippo AD, Novellino L, Castelli C. Unique human tumor antigens: immunobiology and use in clinical trials. J Immunol 2007; 178:1975–9.
4. Vesely MD, Kershaw MH, Schreiber RD, Smyth MJ. Natural innate and adaptive immunity to cancer. Annu Rev Immunol 2011;29:235–71.
5. Boon T, Coulie PG, Van den Eynde BJ, van der Bruggen P. Human T cell responses against melanoma. Annu Rev Immunol 2006;24: 175–208.
6. Matsuzaki J, Gnjatic S, Mhawech-Fauceglia P, Beck A, Miller A, Tsuji T, et al. Tumor-infiltrating NY-ESO-1–specific CD8+ T cells are negatively regulated by LAG-3 and PD-1 in human ovarian cancer. PNAS 2010;107:7875–80.
7. Galon J, Costes A, Sanchez-Cabo F, Kirilovsky A, Mlecnik B, Lagorce-Pagès C, et al. Type, density, and location of immune cells within human colorectal tumors predict clinical outcome. Science 2006;313: 1960–4.
8. Mahmoud SMA, Paish EC, Powe DG, Macmillan RD, Grainge MJ, Lee AHS, et al. Tumor-infiltrating CD8+ lymphocytes predict clinical outcome in breast cancer. J Clin Oncol 2011;29:1949–55.
9. Al-Shibli KI, Donnem T, Al-Saad S, Persson M, Bremnes RM, Busund L-T. Prognostic effect of epithelial and stromal lymphocyte infiltration in non-small cell lung cancer. Clin Cancer Res 2008;14:5220–7.
10. Clemente CG, Mihm MCjr, Bufalino R, Zurrida S, Collini P, Cascinelli N. Prognostic value of tumor infiltrating lymphocytes in the vertical growth phase of primary cutaneous melanoma. Cancer 1996;77: 1303–10.
11. Azimi F, Scolyer RA, Rumcheva P, Moncrieff M, Murali R, McCarthy SW, et al. Tumor-infiltrating lymphocyte grade is an independent predictor of sentinel lymph node status and survival in patients with cutaneous melanoma. JCO 2012;30:2678–83.
12. Zhang L, Conejo-Garcia JR, Katsaros D, Gimotty PA, Massobrio M, Regnani G, et al. Intratumoral T cells, recurrence, and survival in epithelial ovarian cancer. N Engl J Med 2003;348:203–13.
13. Sharma P, Shen Y, Wen S, Yamada S, Jungbluth AA, Gnjatic S, et al. CD8 tumor-infiltrating lymphocytes are predictive of survival in muscle-invasive urothelial carcinoma. PNAS 2007;104:3967–72.
14. Fridman WH, Pagès F, Sautès-Fridman C, Galon J. The immune contexture in human tumours: impact on clinical outcome. Nature Reviews Cancer 2012;12:298–306.
15. Pagès F, Kirilovsky A, Mlecnik B, Asslaber M, Tosolini M, Bindea G, et al. In situ cytotoxic and memory T cells predict outcome in patients with early-stage colorectal cancer. J Clin Oncol 2009;27:5944–51.
16. Mlecnik B, Tosolini M, Kirilovsky A, Berger A, Bindea G, Meatchi T, et al. Histopathologic-based prognostic factors of colorectal cancers are associated with the state of the local immune reaction. J Clin Oncol 2011;29:610–8.
17. Galon J, Pagès F, Marincola FM, Angell HK, Thurin M, Lugli A, et al. Cancer classification using the Immunoscore: a worldwide task force. J Transl Med 2012;10:205.
18. Mellman I, Coukos G, Dranoff G. Cancer immunotherapy comes of age. Nature 2011;480:480–9.
19. Thaunat O, Patey N, Caligiuri G, Gautreau C, Mamani-Matsuda M, Mekki Y, et al. Chronic rejection triggers the development of an aggressive intragraft immune response through recapitulation of lymphoid organogenesis. J Immunol 2010;185:717–28.
20. Carragher DM, Rangel-Moreno J, Randall TD. Ectopic lymphoid tissues and local immunity. Semin Immunol 2008;20:26–42.
21. Neyt K, Perros F, GeurtsvanKessel CH, Hammad H, Lambrecht BN. Tertiary lymphoid organs in infection and autoimmunity. Trends Immunol 2012;33:297–305.
22. GeurtsvanKessel CH, Willart MAM, Bergen IM, van Rijt LS, Muskens F, Elewaut D, et al. Dendritic cells are crucial for maintenance of tertiary lymphoid structures in the lung of influenza virus-infected mice. J Exp Med 2009;206:2339–49.
23. Halle S, Dujardin HC, Bakocevic N, Fleige H, Danzer H, Willenzon S, et al. Induced bronchus-associated lymphoid tissue serves as a general priming site for T cells and is maintained by dendritic cells. J Exp Med 2009;206:2593–601.
24. Perros F, Dorfmüller P, Montani D, Hammad H, Waelput W, Girerd B, et al. Pulmonary lymphoid neogenesis in idiopathic pulmonary arterial hypertension. Am J Respir Crit Care Med 2012;185:311–21.
25. Moyron-Quiroz JE, Rangel-Moreno J, Kusser K, Hartson L, Sprague F, Goodrich S, et al. Role of inducible bronchus associated lymphoid tissue (iBALT) in respiratory immunity. Nat Med 2004;10:927–34.
26. Moyron-Quiroz JE, Rangel-Moreno J, Hartson L, Kusser K, Tighe MP, Klonowski KD, et al. Persistence and responsiveness of immunologic memory in the absence of secondary lymphoid organs. Immunity 2006;25:643–54.
27. Dieu-Nosjean M-C, Antoine M, Danel C, Heudes D, Wislez M, Poulot V, et al. Long-term survival for patients with non-small-cell lung cancer with intratumoral lymphoid structures. J Clin Oncol 2008; 26:4410–7.
28. Miyasaka M, Tanaka T. Lymphocyte trafficking across high endothelial venules: dogmas and enigmas. Nat Rev Immunol 2004;4:360–70.
29. De Chaisemartin L, Goc J, Damotte D, Validire P, Magdeleinat P, Alifano M, et al. Characterization of chemokines and adhesion molecules associated with T cell presence in tertiary lymphoid structures in human lung cancer. Cancer Res 2011;71:6391–9.
30. Detterbeck FC, Boffa DJ, Tanoue LT. The new lung cancer staging system. Chest 2009;136:260–71.
31. Brambilla E, Travis WD, Colby TV, Corrin B, Shimosato Y. The new World Health Organization classification of lung tumours. Eur Respir J 2001;18:1059–68.

32. Altman DG, Lausen B, Sauerbrei W, Schumacher M. Dangers of using "optimal" cutpoints in the evaluation of prognostic factors. J Natl Cancer Inst 1994;86:829–35.
33. Sturn A, Quackenbush J, Trajanoski Z. Genesis: cluster analysis of microarray data. Bioinformatics 2002;18:207–8.
34. Coppola D, Nebozhyn M, Khalil F, Dai H, Yeatman T, Loboda A, et al. Unique ectopic lymph node-like structures present in human primary colorectal carcinoma are identified by immune gene array profiling. Am J Pathol 2011;179:37–45.
35. Moussion C, Girard J-P. Dendritic cells control lymphocyte entry to lymph nodes through high endothelial venules. Nature 2011;479: 542–6.
36. Martinet L, Le Guellec S, Filleron T, Lamant L, Meyer N, Rochaix P, et al. High endothelial venules (HEVs) in human melanoma lesions: major gateways for tumor-infiltrating lymphocytes. Oncoimmunology 2012; 1:829–39.
37. Cipponi A, Mercier M, Seremet T, Baurain J-F, Théate I, Oord J van den, et al. Neogenesis of lymphoid structures and antibody responses occur in human melanoma metastases. Cancer Res 2012;72: 3997–4007.
38. Martinet L, Garrido I, Filleron T, Le Guellec S, Bellard E, Fournie J-J, et al. Human solid tumors contain high endothelial venules: association with T- and B-lymphocyte infiltration and favorable prognosis in breast cancer. Cancer Res 2011;71:5678–87.
39. Hindley JP, Jones E, Smart K, Bridgeman H, Lauder SN, Ondondo B, et al. T-cell trafficking facilitated by high endothelial venules is required for tumor control after regulatory T-cell depletion. Cancer Res 2012;72:5473–82.
40. Thompson ED, Enriquez HL, Fu Y-X, Engelhard VH. Tumor masses support naive T cell infiltration, activation, and differentiation into effectors. J Exp Med 2010;207:1791–804.
41. Schrama D, thor Straten P, Fischer WH, McLellan AD, Bröcker EB, Reisfeld RA, et al. Targeting of lymphotoxin-alpha to the tumor elicits an efficient immune response associated with induction of peripheral lymphoid-like tissue. Immunity 2001;14: 111–21.
42. Yu P, Lee Y, Liu W, Chin RK, Wang J, Wang Y, et al. Priming of naive T cells inside tumors leads to eradication of established tumors. Nat Immunol. 2004;5:141–9.
43. Ruffini E, Asioli S, Filosso PL, Lyberis P, Bruna MC, Macri L, et al. Clinical significance of tumor-infiltrating lymphocytes in lung neoplasms. Ann Thorac Surg 2009;87:365–72.
44. Suzuki K, Kachala SS, Kadota K, Shen R, Mo Q, Beer DG, et al. Prognostic immune markers in non–small cell lung cancer. Clin Cancer Res 2011;17:5247–56.
45. Bos R, Sherman LA. CD4+ T-cell help in the tumor milieu is required for recruitment and cytolytic function of CD8+ T lymphocytes. Cancer Res 2010;70:8368–77.